Tracking atmospheric jets as Lagrangian objects

Louis Rivoire†[a,b,c], Jezabel Curbelo‡[d,e,f], and Marianna Linz[b,c]

[a]Department of Earth, Atmospheric and Planetary Sciences, Massachusetts Institute of Technology, 77 Massachusetts Avenue, Cambridge, MA 02139, USA
[b]Department of Earth and Planetary Sciences, Harvard University, 20 Oxford Street, Cambridge, MA 02138, USA
[c]School of Engineering and Applied Sciences, Harvard University, 29 Oxford Street, Cambridge, MA 02138, USA
[d]Departament de Matemàtiques, Universitat Politècnica de Catalunya, Avd. Diagonal 6447, 08028 Barcelona, Spain
[e]IMTech. Institute of Mathematics, UPC-BarcelonaTech, 08028 Barcelona, Spain
[f]Centre de Recerca Matemàtica, 08193 Bellaterra, Spain

Corresponding authors: † lrivoire@mit.edu, ‡ jezabel.curbelo@upc.edu

Abstract

Accurately determining the position of the upper-tropospheric jets on synoptic scales is key to understanding climate variability and regional weather patterns. However, the conventional Eulerian view of jets tends to overlook their meandering over time, focusing instead on fast and spurious streaks to the detriment of weaker but continuous features that shape large-scale transport. Here, we make the case for a Lagrangian perspective to resolve this issue, defining jets as maxima of quasi-horizontal transport and developing a new identification scheme called 'JetLag.' Applying JetLag to the historical record (1941-2024), we show that the Lagrangian view recovers well-known jet features, with key added benefits; in particular, the new depiction of jet latitude and variability is, on average, virtually insensitive to parameter choice. JetLag further detects strong and weak jets alike, providing continuous jet axes without relying on ad hoc or climatological thresholds. Overall, this study offers a meaningful step toward a unified view of jets across latitudes and climates, achieved without a priori knowledge or sensitivity to method design choices.

Introduction

Jet streams are fundamental organizing features of the atmospheric circulation [1], marking the primary pathways along which synoptic scale disturbances develop and travel, as well as the poleward edge of the Hadley circulation that shapes climatic zones globally. Jets develop near sharp meridional gradients of temperature and exhibit enhanced baroclinicity, that is, potential energy for the development of weather disturbances. The behavior of jets on synoptic scales is therefore intrinsically linked with the weather experienced at the surface, including extreme weather events.

The regional and global response of jets to global warming remains the focus of extensive research. Key topics include the poleward migration of the subtropical jet [2, 3, 4] and possible changes in the midlatitude jet (also referred to as eddy-driven jet or polar-front jet) linked to Arctic warming [5]. However, neither the causes nor magnitudes of these responses are clearly established, owing to discrepancies between methods [4], between models [5], and between models and observations [6], as well as large internal variability [7].

Some of these uncertainties may owe to counteracting drivers of change [8], but discrepancies in our understanding of the jets also arise from discrepancies in the way jet identification algorithms are formulated [9]. Jets are most commonly defined as maxima of instantaneous or time-averaged wind speed (or derivatives, see later discussion); for instance, the glossary of the American Meteorological Society defines jets as "relatively strong winds concentrated within a narrow stream [...]." Synoptic applications of this widely adopted Eulerian definition tend to yield a view of jets as fragmented objects that only manifest when they are distinct enough from some background state, and are then referred to as 'jet streaks.' Zonal mean applications of the definition inevitably smooth the jet over a wide range of latitudes, thus masking the effects of narrow bands of high winds.

One of the key characteristics of jets is their role as mixing barriers [e.g., 10, 11, 12, 13, 14], with implications for transport processes [15, 16, 14] that play a key role in setting midlatitude temperature distributions [17, 18]. In attempting to improve upon existing jet identification schemes, our goal is thus to develop a robust method that reflects the role of jets as transport barriers.

Consequences of Eulerian Methods. We highlight several key issues that arise from the Eulerian view of jets. First, discrete jet streaks can be associated with ageostrophic disturbances [1], and while important for weather system development [19], are more directly relevant to vertical motion and precipitation processes [20, 21] or tropopause folding in baroclinic regions [22] than they are to synoptic transport and horizontal mixing. Indeed, spurious wind maxima can differ from maxima in synoptic transport (see Fig. 1B); for instance, a "large-amplitude orographic wave could be recorded as a jet [...] even in the absence of a coherent and elongated jet stream" [23]. Conversely, regions with low wind speeds–though capable of supporting long-range transport–may be overlooked in jet diagnostics (see Fig. 1C).

Second, unless jet streaks are continuously tracked over time, nothing precludes a jet from being assigned to very different locations from one time step to the next. Regions with dual jets or frequent wave breaking, which are of notable interest to the scientific community, are particularly prone to this issue. There, jets often appear as disjointed collections of streaks that enter and exit the phase space at nonphysical speeds. Such behavior is expected to affect the representation of synoptic variability in jet diagnostics, with important implications for mean jet characteristics [e.g., 4].

Third, algorithms formulated to locate jet streaks within specified domains–whether 2- or 3-dimensional–tend to rely on a variety of *ad hoc* parameters chosen to produce the desired output. For instance, a wind speed threshold commonly serves as minimum condition to define jets from daily or 6-hourly model output [24, 25, 23, 26, 27, 28, 2, 29]. While strong and steady jets are easily located with this approach, weaker portions of the jets can be overlooked, potentially excluding those associated with blocking patterns and extreme events. If the phase space is truncated, jet variability is also likely misrepresented. In addition, the minimum wind threshold used varies across even closely related studies, alternatively 25.7 $m\ s^{-1}$ [24, 25], 30 $m\ s^{-1}$ [23, 26, 27], or 40 $m\ s^{-1}$ [28, 2] for the subtropical jet. The sensitivity of the output to these changes is difficult to quantify because a variety of other parameters are frequently used [see 4, Table 1].

Last, parameter choice is often based on a priori climatological knowledge. For instance, the 30 $m\ s^{-1}$ isotach in the upper troposphere, or the 100-400 hPa layer both describe volumes within which the subtropical jets are expected to be located. The use of such constraints greatly simplifies tracking algorithms, but it also tailors their skill to the current state of the climate system. Such algorithms should not be assumed to be suitable for the analysis of long-term changes and for comparisons across datasets [30, 4].

In the quest to address the issues outlined above, some studies have turned to alternative definitions of the jets: as zero crossings of the wind shear [31, 32], as circumpolar isolines of the upper tropospheric streamfunction [33], accounting for mass-flux rather than wind alone [34], as maxima of meridional gradient of potential temperature along the tropopause [4], or using integrated quantities to overcome the jets' noisy nature [34]. However, the issue of *ad hoc* parameters and sensitivities thereto remains, and the majority of methods remain Eulerian in nature and prone to the issues discussed above.

We propose a Lagrangian view of jets to address these issues. A key motivation to adopt a Lagrangian view stems from jets being regions of organized shear flow that resist rapid mixing with surrounding fluid. As such, jets produce coherent transport over large scales, effectively dividing the phase space into regions with different dynamical fates. Jets act as transport barriers [11, 35, 36, 37, 38, 12], that is, "material surface[s] that [remain] coherent by withstanding stretching and filamentation" [12]. This conceptual view allows Lagrangian jets to be unsteady while maintaining their structural integrity and function over time. We propose an alternative Lagrangian definition of jets as transport maxima (see Fig. 1A) and showcase its capabilities.

Results

We devise a new Lagrangian algorithm called 'JetLag' (for LAGrangian JET) which defines jets as the most salient *and* most connected synoptic transport features in the upper troposphere. JetLag computes jet coordinates using the Lagrangian descriptor called $\mathcal{M}$, which is the length of massless parcel trajectories integrated τ days both forward and backward in time (see Materials and Methods). For the proof of concept, we apply the method to the ERA5 wind field along two isentropic surfaces, 350 K and 315 K, to locate the subtropical jet (STJ) and polar-front jet (PFJ), respectively. The choice of isentropic surfaces is based on the bimodal distribution of upper tropospheric jets [28, 39]. The assumption of isentropic motion is discussed in the Materials and Methods and Supplementary Materials (Figs. S3-S5).

Performance and sensitivity of the algorithm

We test JetLag for the STJ against two reference Eulerian definitions: 1) as a maximum of wind speed near the subtropical tropopause drop, and 2) as the tropopause drop itself. The first concept is implemented using an adaptation of Manney et al. [28] and Manney and Hegglin [2] and is referred to as the 'wind-based' method. The second is implemented following Maher et al. [4] and referred to as the 'θ-based' method. Both original methods are adapted to our specific needs because our goal is to compare Eulerian and Lagrangian concepts rather than specific methods. Both comparison algorithms define the STJ as a maximum of a pre-defined metric at each longitude, when applicable (see Methods), with a key difference: the wind-based method truncates the phase space by defining jets only above a pre-determined minimum wind speed threshold (40 $m\ s^{-1}$), while the θ-based method does not.

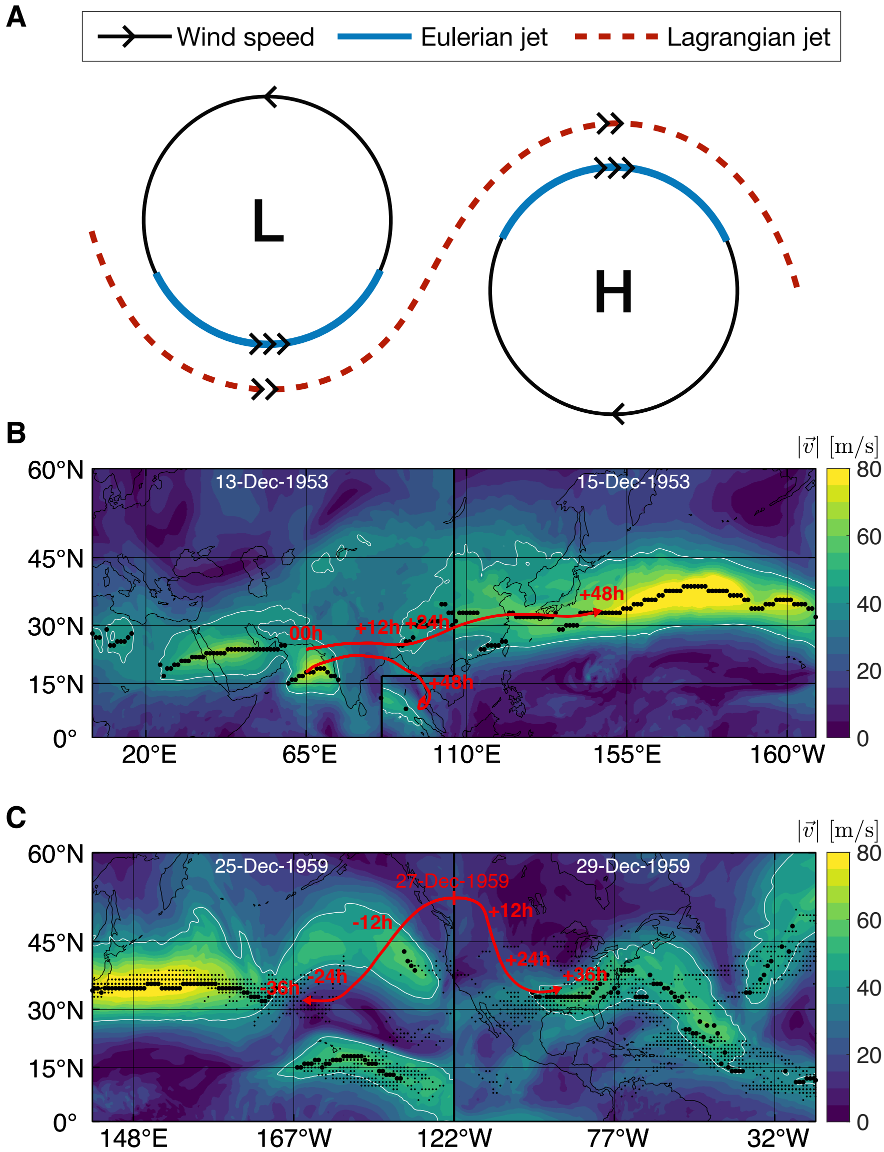

Figure 1: (A) Schematic comparing the Eulerian (wind-based) and Lagrangian (transport-based) definitions of jets around low (L) and high (H) pressure systems, with arrows representing relative wind speeds. (B,C) Issues arising when tracking the subtropical jet as Eulerian wind maxima (black dots). (B) A portion of the East Asian subtropical jet near 65^{o}E, 18^{o}N is associated with transport pathways (red arrows) that rapidly exit the jet, while nearby pathways starting 600 km north remain within the jet over 10000 km. (C) The subtropical jet in the East Pacific during the time period 25-29 December 1959 (small black dots) exhibits a persistent 7000 km-long gap, but transport pathways exist that bridge this gap over the same time period, implying that mass transport by a relatively weak jet followed a poleward excursion up to 52^{o}N before rejoining the North Atlantic jet.

The choice of integration time τ used for JetLag is based on a simple argument using the Rossby wave dispersion relation (see Eq. 1 in Methods), and τ is therefore a function of zonal wavenumber and latitude (Fig. 2C). The primary modes of variability in the jet correspond to wavenumbers 1-5 [40]. Larger wavenumbers are known to be less stable [41], but they nonetheless contribute to short-term variability. Choosing $\tau = 3$ days allows us to capture wavenumbers 1-10 over latitudes 20-40°, while avoiding excessively large wavenumbers that yield noisy features and complicate the detection of the jet. At higher latitudes, Rossby wave propagation is weaker and only the largest zonal wavenumbers reach the polar regions [42]. For this reason, and for simplicity, we use $\tau = 3$ days for the detection of the STJ and PFJ alike.

The Lagrangian descriptor integrated for 3 days (Fig. 2A) clearly exhibits a circumpolar maximum at 350 K, which the detection algorithm identifies. Lagrangian and Eulerian jet axes can exhibit significant differences even in regions where strong and steady winds are typically found (e.g., Western Pacific in Northern Hemisphere winter, Fig. 2B).

However, in these regions, the Lagrangian jet exhibits remarkable stability to changes in the Lagrangian descriptor's integration time (Fig. 2D), consistent with Mancho et al. [43]: on average, changing the integration time by as much as 66% (from 3 days) changes the location of the Lagrangian STJ by less than 0.1 degree. In contrast, the location of the wind-based STJ is over fifty times more sensitive to changes in the wind speed threshold: a mere 25% change (from 40 $m\ s^{-1}$) shifts the mean latitude of the STJ by ∼2 degrees. Minimal sensitivity in the Lagrangian jet is confined to regions of Rossby wave breaking (indicated by gamma-shaped features in $\mathcal{M}$ like the one near 135°W in Fig. 2A, also see Mancho et al. [43]). We note that the leveling off in the sensitivity of the wind-based method at high wind speed thresholds in summer is an indicator of extreme truncation of the phase space rather than robustness of the wind-based method. These results highlight the versatility of our Lagrangian framework and its robustness to parameter choice, demonstrating that JetLag can be a reliable tool to track jets in highly dynamic regions.

Jet climatology

Spatial distributions of STJ occurrence in DJF for JetLag and the wind-based method are shown in Fig. 3A and B, respectively. JetLag recovers familiar features broadly matching waveguides predicted by Rossby wave theory [44] and identified by Eulerian methods [e.g., 23, 28, 27, 32]: the Asian STJ (from Northern Africa to the Western Pacific) and North Atlantic STJ (from North America to Western Europe), as well as the North Atlantic and Pacific storm tracks. Some differences are visible in the mean, as shown in Fig. 3C: in regions where Rossby wave breaking is common (Eastern Pacific, North Atlantic), JetLag is able to assign a coherent structure to the STJ more often than the wind-based method, as expected from Fig. 1C. Differences in the mean latitude of the frequency maximum also imply that synoptic transport tends to maximize poleward of the wind-based jet in winter. Lastly, the wind-based method's output is affected by salient mountain ranges (Himalayas, Sierra Madre, Zagros Mountains), as discussed previously, while JetLag is not.

The occurrence frequency and mean position of the PFJ in DJF for JetLag is shown in Fig. 3D. Strong zonal asymmetry is visible, most notably the tilt of the North Atlantic storm track. Features are in qualitative agreement with those seen in analysis of the PFJ on a lower tropospheric isentrope [39]. Jet occurrence exhibits a single maximum in the

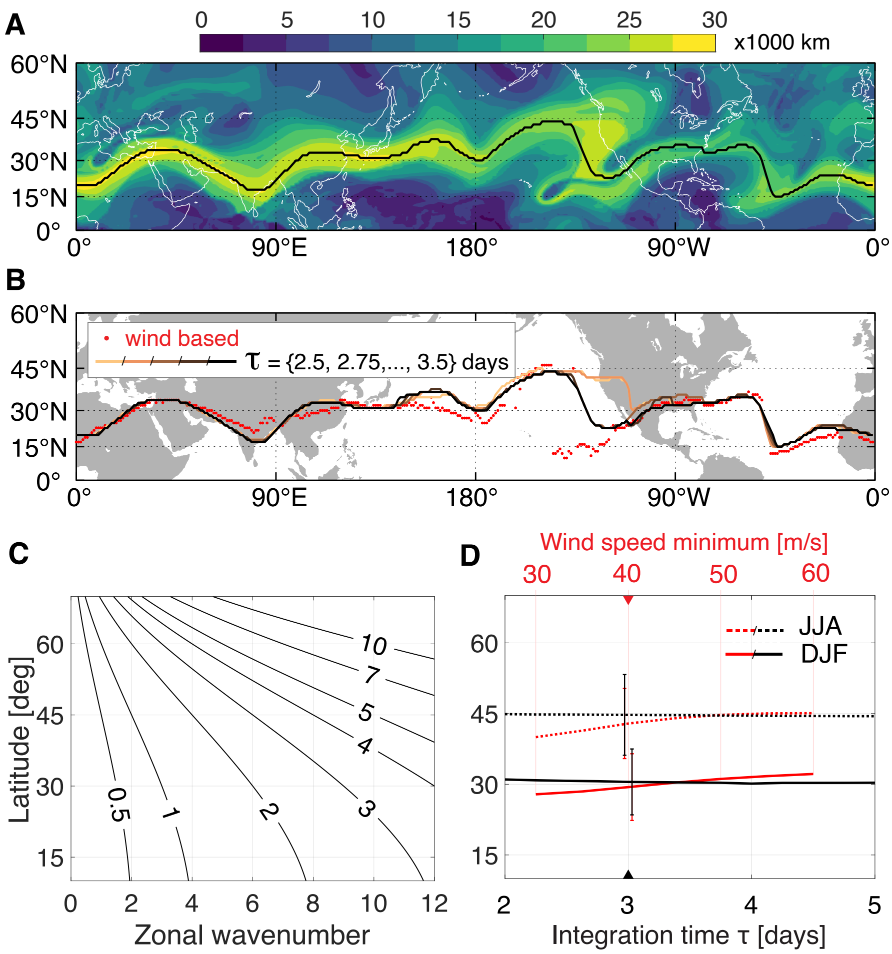

Figure 2: (A) Lagrangian descriptor $\mathcal{M}$ integrated for 3 days (shading) and position of the corresponding Lagrangian jet (black) on 2020-01-01 at 350 K. (B) Comparison between the wind-based jet (red dots) and Lagrangian jets (solid lines) calculated for five integration times from 2.5 to 3.5 days in 6-hour increments. (C) Integration time (in days) for a range of wavenumbers and latitudes, corresponding to Eq. 1. (D) Sensitivity of the mean latitude of the Northern Hemisphere subtropical jet to changes in integration time and in the wind minimum threshold. Horizontal axes are scaled so that relative departures from reference points (colored triangles) are equal. Error bars show ±1 standard deviation of the mean.

North Atlantic rather than the multimodal distribution previously thought to indicate regime behavior [45]. This result is in agreement with recent literature highlighting the role of orography, rather than large-scale variability, in setting the northern peak in the Eulerian distribution of the PFJ [46]. This result also confirms our conceptual view of Lagrangian jets in Fig. 1A: the continuity of the jet axis is prioritized over intermittent and local acceleration in the wind field.

Distributions in Fig. 3E-F highlight that, in the statistical sense, similarities in the latitudinal position of jet features across methods are not mutually exclusive with marked discrepancies in wind speeds. In other words, collections of features that make up the zonal mean may average to similar latitudes but capture different wind speeds. Since JetLag and the θ-based method are not constrained by the 40 $m\ s^{-1}$ minimum wind speed threshold, it is not surprising that their output can capture lower wind speeds than the wind-based method.

Jet variability

Hovmöller diagrams in Fig. 4A demonstrate the superior detection power of JetLag over the wind-based method for wave structures; both methods capture the most salient waves, but JetLag is able to complete the picture with features associated with relatively weak winds. This is particularly true of regions of frequent Rossby wave breaking, as illustrated in Fig. 1C. The θ-based method (not shown) provides continuous jet axes but captures features with weaker meridional wind speeds, yielding less distinct (and noisier) wave structures.

Time series in Fig. 4B-C highlight again that jet properties can differ vastly even when their zonal mean latitude is fairly consistent between methods. JetLag and the θ-based method exhibit a seasonal cycle with larger amplitude in the wind speed. Even in winter, wind speeds near Lagrangian jets are not quite as large as those near wind-based jets, consistent with the conceptual view in Fig. 1.

Based on power spectra in Fig. 4D, the two Eulerian jet definitions yield more short-term variability in the zonal mean jet latitude than JetLag does. The difference is attributable to fast, non-physical transition between Eulerian jet streaks, which is a prominent issue in summer. Since JetLag relies on a multi-day history of the wind field to locate the jet, it is less subject to this issue. Short-term variability in the wind-based method is also influenced by regions where wind speeds fall below the detection threshold. JetLag further yields elevated power on decadal to multidecadal scales: for reference, the integrated power for periods longer than 10 years is three times larger with JetLag than with the wind-based method. We attribute this difference to JetLag's global perspective on jets, compared to the more regional focus of Eulerian methods; by following air parcels, the Lagrangian view captures the influence of interactions across scales including those bearing the structural imprint of low-frequency modes. That said, the magnitude of multidecadal variability remains uncertain, both because the historical record is relatively short, and because of parameter sensitivity. For instance, increasing the wind speed threshold of the wind-based method from 30 $m\ s^{-1}$ to 60 $m\ s^{-1}$ triples the integrated power estimate for periods longer than 10 years (and nearly halves variability on timescales associated with El Niño Southern Oscillation, 3 to 5 years). Changing the degree of the polynomial used in the θ-based method also affects long-term variability. In comparison, JetLag is virtually insensitive to changes in its parameters.

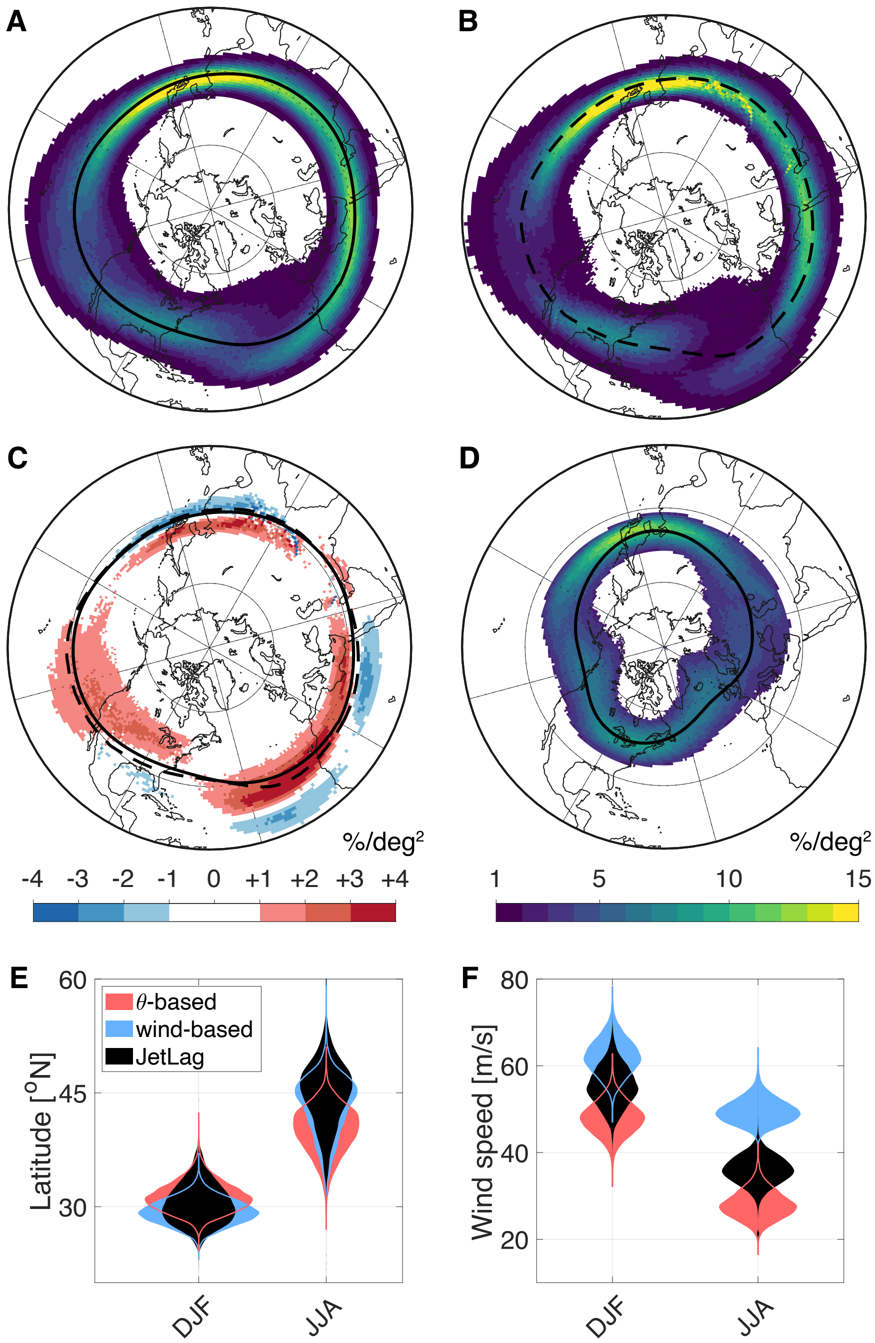

Figure 3: Occurrence frequency of the STJ in DJF using (A) JetLag, (B) the wind-based method, and (C) the difference between the two in that order (A minus B). (D) PFJ in DJF using JetLag. Frequencies are percentages of the time normalized by surface area. The mean position of jets appears as thick black lines (dashed and solid), and latitude circles are shown at 30^{o}N and 60^{o}N. (E-F) Distributions of zonal mean Northern Hemisphere STJ latitude and wind speed. All data are from ERA5 1941-2024.

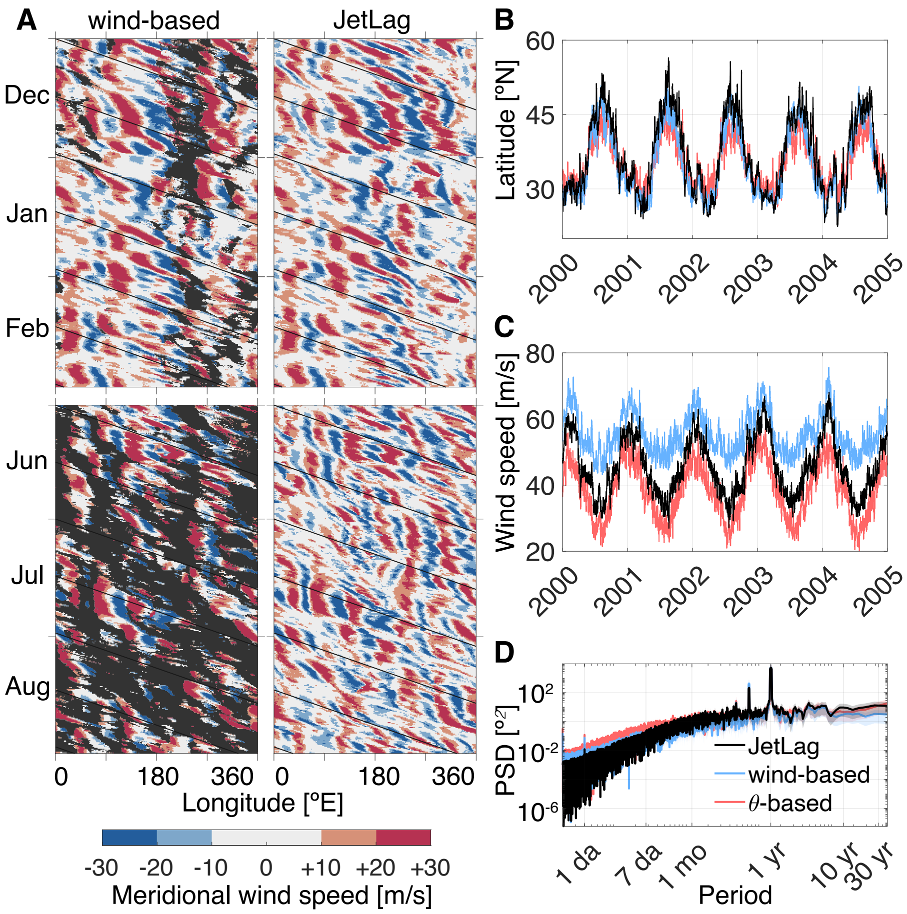

Figure 4: (A) Space-time diagrams of the meridional component of the wind along the 1999-2000 Northern Hemisphere STJ axis, with missing data grayed out and black lines indicating 25 $m\ s^{-1}$ zonal propagation speed. (B-C) Sample time series of the 6-hourly zonal mean jet latitude and wind speed. (D) Power spectral density of the same quantity as in (B) for 1941-2024, shown with a 95% confidence interval calculated with multitapers. Total power is comparable between methods.

Discussion

We investigated the upper tropospheric jets through the lens of synoptic-scale transport, with the goal of developing a generally applicable diagnostic for their position. Overall, our results motivate the use of an alternate definition of jets as maxima of Lagrangian descriptors of synoptic transport. Our algorithm, called JetLag, captures jets as continuous, physically grounded features that exhibit the spatial and temporal coherence characteristic of synoptic-scale flow. The jet axes identified by JetLag are suitable for studies in jet-relative coordinates, wavenumber decomposition, regional trend analyses, etc. Given the influence of synoptic variability on the position of the jets [4], our approach could effectively complement existing Eulerian methods that have a propensity to truncate the phase space and capture disconnected features with behavior sometimes beyond physically reasonable limits.

Tracking coherent features, rather than eddy-related features, may also be a useful approach to quantify the response of jets to wave forcing: if jet waveguideability (in the zonal mean sense) is a consequence of wave activity rather than a precondition for it [47], then identifying and following coherent jet structures may offer a clearer view of how wave forcing influences jets (including persistent weather patterns, teleconnections between tropics and midlatitudes, changes in storm tracks, etc).

By relying on only two physically grounded parameters, JetLag also addresses the longstanding shortcoming of the reliance on *ad hoc* or climatology-based parameters. Indeed, the Lagrangian descriptor we use provides a relatively simple and uniform description of jets at all latitudes, with little sensitivity to its integration time. JetLag is therefore well suited to the study of long-term trends and their uncertainties. Even though model uncertainties largely contribute to uncertainties in future trends in the jets [6, 4, 48, 49], decreasing method uncertainty is also important since methods differ in their representation of jet variability and mean characteristics. Indeed, trend analyses are heavily influenced by the spectrum of variability in the variables of interest, and artificial trends can also arise from the design of methods itself [50, 51].

In its current form, our algorithm identifies one jet axis at a time, precluding the explicit detection of split jet states. Of two branches, JetLag selects the one which is best connected to the broader pattern of zonal transport. Though the algorithm could be modified to detect persistent splits in the jets, a robust framework to understand such structures from the Lagrangian perspective is needed first. We leave these developments to future work, along with potential adaptations to capture recurving jet features that go beyond the one-latitude-per-longitude simplification used in the present approach.

While JetLag has the desirable characteristic of being virtually insensitive to the choice of its parameters, the choice of isentropic surface along which it is applied yields different results–which we leverage to distinguish the STJ and PFJ. If the thermal structure of near-tropopause levels changes over time, then the choice of isentrope should also change to avoid artificial trends; indeed, an increasing height of the tropopause with global warming is thought to drive shifts in the wind field in the mid- and upper troposphere [52]. With appropriate isentropic levels, JetLag's non-reliance upon climatology-based parameters should enable comparisons of jet variability and position in vastly different model runs, including idealized setups, climate projections under various emissions scenarios, and other planetary atmospheres in general. Such model analysis is an exciting avenue for future work to better understand how jets will change with global warming.

Materials and Methods

Lagrangian descriptor

We use the quantity known as $\mathcal{M}$ [53, 54, 43] to diagnose jets as coherent maxima of parcel displacement. The function $\mathcal{M}$ is a heuristic which associates to initial conditions in space $\mathbf{x}^*$ and time t^* the arc length of the trajectory initiated with those conditions and integrated backwards and forwards in time over the interval $[t^* - \tau; t^* + \tau]$:

$$\mathcal{M}(\mathbf{x}^*, t^*, \tau) = \int_{t^*-\tau}^{t^*+\tau} \sqrt{\sum_{i=1}^{n} \left(\frac{d\mathbf{x}_i(t)}{dt}\right)^2} dt$$

with $\mathbf{x}(t)$ trajectories of the system:

$$\begin{aligned} \frac{d\mathbf{x}}{dt} &= \mathbf{v}(\mathbf{x}, t) \\ \mathbf{x}(t^*) &= \mathbf{x}^* \end{aligned}$$

with $\mathbf{v}$ the vector field of velocity with n components. See Mancho et al. [43] for details. Unlike an Eulerian average of the flow field, the descriptor $\mathcal{M}$ does not smooth features and reveals sharper features as τ increases; large-scale features in $\mathcal{M}$ are established at short integration times and do not fundamentally change as the integration time is increased. This property is illustrated in the Supplementary Materials, both for a simple flow (an idealized vortex embedded in a purely zonal flow, Fig. S1) and for a real case (Fig. S2).

Calculating $\mathcal{M}$ requires calculating parcel trajectories, which we assume travel along isentropic surfaces. This assumption reflects the expectation that, on the scales of interest, quasi-balanced dynamics dominate over diabatic effects such as latent heat release and cloud-radiative forcing. Indeed, particles released in the extratropical middle and upper troposphere are known to disperse much faster along isentropes than across them [e.g., 55, 56, 57]. That being said, parcels in transit may encounter a range of net heating rates along their trajectories, and do so in a seasonally dependent manner that is reflected in the $\mathcal{M}$ descriptor. We provide three figures and a discussion in the Supplementary Materials to illustrate this point and confirm that ignoring the local influence of non-conservative processes is not expected to systematically reshape the dominant structures captured by the $\mathcal{M}$ descriptor on planetary scales. Further, the sensitivity of the jet axis to non-conservative effects on smaller scales is mitigated by the 1 degree horizontal resolution used for trajectory integration and by the detection algorithm's robustness to noise (see Jet detection algorithm); jet axes are generally only affected if non-conservative processes act to consistently displace local maxima of $\mathcal{M}$ on spatial scales close to the Rossby radius of deformation. Figures S3-S5 in the Supplementary Materials show the extent to which this assumption affects the position of the jet axis.

Trajectories are calculated along 350 K for the STJ and 315 K for the PFJ, given jet occurrence frequencies in previous literature [e.g., 28, 39]. The wind field used to calculate trajectories is from the European Centre for Medium-Range Weather Forecasts' ERA5 reanalysis, provided at a 6-hourly frequency and integrated hourly with a fifth-order Cash-Karp Runge–Kutta scheme as in Curbelo et al. [58].

Setting the integration time

The time interval $[t^* - \tau; t^* + \tau]$ used to calculate $\mathcal{M}$ is the time period during which the features defined by the $\mathcal{M}$ function are coherent. Within jets, such features are primarily shaped by Rossby waves. We therefore relate τ to the intrinsic period of Rossby waves, written as the inverse of their intrinsic frequency:

$$2\tau \equiv \left|\frac{1}{\hat{\omega}}\right|$$

where the factor 2 arises from the integration interval including both forward and backward direction. The intrinsic period is related to wave properties by the dispersion relation:

$$\hat{\omega} = -\frac{\beta k}{k^2 + l^2}$$

where β is the Rossby parameter, k and l are the zonal and meridional wavenumbers. Focusing on the zonal structure of waves, we assume $l^2 \ll k^2$ and arrive to:

$$\tau = \left|-\frac{k}{2\beta}\right| \tag{1}$$

The sensitivity of our method to the choice of integration time is illustrated in Fig. 2D.

Jet detection algorithm

Jets are defined as connected local maxima (that is, ridges) of $\mathcal{M}$. A number of approaches exist to extract ridges from 2D data, ranging from simple gradient-based and edge detection methods to more complex morphological operations, such as watershed and wavelet transforms. We choose an algorithm with a good trade-off between complexity and performance.

The axis of the jet is defined at each longitude using a penalized forward-backward greedy algorithm. Using a greedy heuristic allows us to avoid defining the jet axis merely as the maximum of $\mathcal{M}$ at each longitude; the algorithm penalizes large changes in latitude from one longitude to the next, so as to prioritize following continuous features rather than overfitting to large values of $\mathcal{M}$. In order to further focus on large-scale patterns, the dynamic range in values of $\mathcal{M}$ is decreased by taking its negative natural logarithm. We note that minimizing $-\log \mathcal{M}$ is equivalent to maximizing $\mathcal{M}$.

During the forward pass, the greedy algorithm steps through adjacent meridians and calculates updated values of $-\log \mathcal{M}$ by adding to them a penalty as follows:

$$-\log \mathcal{M} + p \times \text{dist}^2$$

with p the penalty parameter and dist the distance between any two latitudinal positions for adjacent meridians. This formula is applied longitude by longitude from west to east ("forward") for all latitudes, keeping track of the latitudinal positions which produce the smallest updated values. The algorithm then does a second pass from east to west ("backward"), tracing the path corresponding to the latitudes with the smallest updated values (and therefore, the largest *and* most connected values of $\mathcal{M}$).

We provide a simple example to illustrate the process, for a matrix with three latitude bins (rows) across three longitude bins (columns). Consider the matrix of negative logarithmic values:

$$\begin{bmatrix} 1 & 5 & 4 \\ 2 & 1 & 2 \\ 4 & 5 & 5 \end{bmatrix}$$

The forward pass is applied to each column using the elements of the column immediately to its left. Starting with the first element of column 2, that is, element (1,2), and applying a penalty of value 1 (for the sake of example) to the elements of column 1 based on their distance from element (1,2), column 1 becomes:

$$\begin{aligned} 1 + 1 \times 0^2 &= 1 \\ 2 + 1 \times 1^2 &= 3 \\ 4 + 1 \times 2^2 &= 8 \end{aligned}$$

Comparing these values with the original 2nd column:

$$\begin{matrix} 1 & 5 \\ 3 & 1 \\ 8 & 5 \end{matrix}$$

The minimum value of the updated column is 1 in row 1. It is added to original element (1,2), which becomes $6_{(1)}$ to denote that this value came from row 1. Elements (2,2) and (3,2) are updated using the same process, and the algorithm proceeds to column 3, this time applying the penalty formula to the updated second column. The updated matrix contains the penalized values along with their row of origin from the preceding longitude bin:

$$\begin{bmatrix} 1 & 6_{(1)} & 8_{(2)} \\ 2 & 3_{(2)} & 5_{(2)} \\ 4 & 8_{(2)} & 9_{(2)} \end{bmatrix}$$

To find the most salient ridge, the greedy algorithm starts from the last column and traces backward through the matrix, following the origin of the minimum value in each column. In our example, element (2,3) is the minimum ($5_{(2)}$) in column 3, so the ridge is at row 2 in column 3. Since $5_{(2)}$ came from row 2, the ridge location is row 2 at column 2. In column 2, the value at row 2 ($3_{(2)}$) came from row 2 as well, so the ridge is also located at row 2 in column 1.

Since this greedy algorithm is designed to extract a unique ridge, split jet states or synoptic situations with multiple transport pathways in general will be reduced to one pathway: that which is most connected to the broader pattern of zonal transport. In the hypothetical case where multiple pathways are equally well connected, the algorithm defaults to selecting the one with smaller meridional excursions.

In order to ensure periodicity in the $\mathcal{M}$ ridge, the algorithm is applied five times, cyclically shifting its longitude coordinates to evaluate the output across five randomly selected longitudinal starting points. The final output is constructed by selecting, at each longitude, the latitude most frequently identified as ridge across the five iterations. This procedure guarantees that the output is periodic and therefore unaffected to the choice of starting longitude. In practice, this procedure rarely alters the output by more than a single grid cell, thanks to the algorithm's ability to identify dominant features with greedy logic.

The value of the penalty parameter p is chosen based on the typical scale of Rossby waves. With a 3-day integration time, assuming maximum wind speeds of order 100 $m\ s^{-1}$, maximum values of $\mathcal{M} \sim 3 \times 10^4$ km are expected corresponding to $-\log \mathcal{M}$ ~-10. Given the penalty formula, p needs to be chosen so that updated values of $-\log \mathcal{M}$ at the largest allowed latitudinal jump become so large they are ruled out by the algorithm:

$$p \times \text{dist}_{max}^2 \sim 10$$

with dist_{max} the largest allowed latitudinal jump between two adjacent longitudes. Interpreting jumps as the crest-to-trough distance within Rossby waves, a reasonable range for dist_{max} is twice the Rossby radius ~2000-4000 km or 18-36 degrees, yielding $p \sim 0.01$. By design, the sensitivity of the jet output to the specific value of p is small: halving or doubling it only changes the average output at a rate of ~0.00001 degree per percent change in p. In addition, any sensitivity to p is confined to sharp features corresponding to wave breaking.

We use MATLAB's implementation of the greedy algorithm, called *tfridge*, which was developed as a signal processing tool.

Eulerian jet metrics

We compare the output of JetLag for the subtropical jet to two Eulerian methods inspired by the JEt and Tropopause Product for Analysis and Characterization (JETPAC) software [28, 2], referred to as 'wind-based' method, and by Maher et al. [4], referred to as 'θ-based' method.

The wind-based method is a 2D adaptation of the 3D algorithm described in Manney and Hegglin [2]. For comparability with JetLag, the wind-based method defines the subtropical jet axis at each longitude as the latitude of maximum wind speed on the 350 K surface, with the same criteria as Manney and Hegglin [2]: that 1) the wind speed is greater than 40 $m\ s^{-1}$, 2) the altitude of the dynamical tropopause (2 PVU surface) at the equatorward edge of the jet (defined as the 30 $m\ s^{-1}$ isotach crossing as in Manney and Hegglin [2]) is greater than 13 km, and 3) the altitude of the dynamical tropopause decreases by at least 2 km from the equatorward to the poleward edge of the jet. We test the sensitivity of this method to the choice of minimum wind speed threshold (Fig. 2D). We choose this method as a point of comparison because using the wind field to define jet metrics is common practice, since climate models provide it as standard output.

The θ-based method is implemented following Maher et al. [4]: the axis of the STJ is defined at each longitude as the largest local maximum in the meridional gradient of potential temperature (θ) along the dynamical tropopause (defined as the $\pm$2 PVU surface). The meridional gradient is calculated using a Chebyshev polynomial of degree 6 between 10^o and 65^o latitude. The differences with Maher et al. [4] are 1) that we use 6-hourly data rather than daily or monthly averaged data (to match JetLag), and 2) that if multiple local maxima in the potential temperature gradient exist (e.g., STJ and PFJ), we simply retain the largest one. We choose this option because we find that applying the vertical wind shear criterion used to separate STJ from PFJ in Maher et al. [4] to instantaneous meteorological fields yields large and spurious excursions in the STJ.

References

[1] James R Holton. An introduction to dynamic meteorology. *American Journal of Physics*, 41(5):752–754, 1973.

[2] Gloria L Manney and Michaela I Hegglin. Seasonal and regional variations of long-term changes in upper-tropospheric jets from reanalyses. *Journal of Climate*, 31(1): 423–448, 2018.

[3] Molly E Menzel, Darryn Waugh, and Kevin Grise. Disconnect between hadley cell and subtropical jet variability and response to increased co2. *Geophysical Research Letters*, 46(12):7045–7053, 2019.

[4] Penelope Maher, Michael E Kelleher, Philip G Sansom, and John Methven. Is the subtropical jet shifting poleward? *Climate Dynamics*, 54(3-4):1741–1759, 2020.

[5] Elizabeth A Barnes and James A Screen. The impact of arctic warming on the midlatitude jet-stream: Can it? has it? will it? *Wiley Interdisciplinary Reviews: Climate Change*, 6(3):277–286, 2015.

[6] Tim Woollings and Mike Blackburn. The north atlantic jet stream under climate change and its relation to the NAO and EA patterns. *Journal of Climate*, 25(3): 886–902, 2012.

[7] Paul W Staten, Jian Lu, Kevin M Grise, Sean M Davis, and Thomas Birner. Re-examining tropical expansion. *Nature Climate Change*, 8(9):768–775, 2018.

[8] Tiffany A Shaw. Mechanisms of future predicted changes in the zonal mean mid-latitude circulation. *Current Climate Change Reports*, 5(4):345–357, 2019.

[9] Tom Keel, Chris Brierley, and Tamsin Edwards. jsmetrics v0. 2.0: a python package for metrics and algorithms used to identify or characterise atmospheric jet streams. *Geoscientific Model Development*, 17(3):1229–1247, 2024.

[10] JD Mahlman. Dynamics of transport processes in the upper troposphere. *Science*, 276(5315):1079–1083, 1997.

[11] FJ Beron-Vera, Michael G Brown, MJ Olascoaga, Irina I Rypina, H Kocak, and Ilya A Udovydchenkov. Zonal jets as transport barriers in planetary atmospheres. *Journal of the atmospheric sciences*, 65(10):3316–3326, 2008.

[12] Alireza Hadjighasem and George Haller. Geodesic transport barriers in jupiter's atmosphere: A video-based analysis. *Siam Review*, 58(1):69–89, 2016.

[13] Ru Chen and Stephanie Waterman. Mixing nonlocality and mixing anisotropy in an idealized western boundary current jet. *Journal of Physical Oceanography*, 47(12): 3015–3036, 2017.

[14] Jezabel Curbelo, Gang Chen, and Carlos Roberto Mechoso. Lagrangian analysis of the northern stratospheric polar vortex split in april 2020. *Geophysical Research Letters*, 48(16):e2021GL093874, 2021.

[15] Chaim I Garfinkel and Nili Harnik. The non-gaussianity and spatial asymmetry of temperature extremes relative to the storm track: The role of horizontal advection. *Journal of Climate*, 30(2):445–464, 2017.

[16] Marianna Linz, Gang Chen, and Zeyuan Hu. Large-scale atmospheric control on non-gaussian tails of midlatitude temperature distributions. *Geophysical Research Letters*, 45(17):9141–9149, 2018.

[17] Talia Tamarin-Brodsky, Kevin Hodges, Brian J Hoskins, and Theodore G Shepherd. A dynamical perspective on atmospheric temperature variability and its response to climate change. *Journal of Climate*, 32(6):1707–1724, 2019.

[18] Boer Zhang, Marianna Linz, and Gang Chen. Interpreting observed temperature probability distributions using a relationship between temperature and temperature advection. *Journal of climate*, 35(2):705–724, 2022.

[19] Louis W Uccellini and Paul J Kocin. The interaction of jet streak circulations during heavy snow events along the east coast of the united states. *Weather and Forecasting*, 2(4):289–308, 1987.

[20] Andrew F Loughe, Chung-Chieng Lai, and Daniel Keyser. A technique for diagnosing three-dimensional ageostrophic circulations in baroclinic disturbances on limited-area domains. *Monthly weather review*, 123(5):1476–1504, 1995.

[21] Deborah Hanley, John Molinari, and Daniel Keyser. A composite study of the interactions between tropical cyclones and upper-tropospheric troughs. *Monthly weather review*, 129(10):2570–2584, 2001.

[22] Matthew S Wandishin, John W Nielsen-Gammon, and Daniel Keyser. A potential vorticity diagnostic approach to upper-level frontogenesis within a developing baroclinic wave. *Journal of the atmospheric sciences*, 57(24):3918–3938, 2000.

[23] Patrick Koch, Heini Wernli, and Huw C Davies. An event-based jet-stream climatology and typology. *International Journal of Climatology: A Journal of the Royal Meteorological Society*, 26(3):283–301, 2006.

[24] J Degirmendžić and J Wibig. Jet stream patterns over europe in the period 1950–2001–classification and basic statistical properties. *Theoretical and applied climatology*, 88:149–167, 2007.

[25] Courtenay Strong and Robert E Davis. Variability in the position and strength of winter jet stream cores related to northern hemisphere teleconnections. *Journal of Climate*, 21(3):584–592, 2008.

[26] Reinhard Schiemann, Daniel Lüthi, and Christoph Schär. Seasonality and interannual variability of the westerly jet in the tibetan plateau region. *Journal of climate*, 22(11):2940–2957, 2009.

[27] Cristina Pena-Ortiz, David Gallego, Pedro Ribera, Paulina Ordonez, and Maria Del Carmen Alvarez-Castro. Observed trends in the global jet stream characteristics during the second half of the 20th century. *Journal of Geophysical Research: Atmospheres*, 118(7):2702–2713, 2013.

[28] GL Manney, Michaela I Hegglin, WH Daffer, ML Santee, EA Ray, S Pawson, MJ Schwartz, CD Boone, L Froidevaux, NJ Livesey, et al. Jet characterization in the upper troposphere/lower stratosphere (utls): applications to climatology and transport studies. *Atmospheric Chemistry and Physics*, 11(12):6115–6137, 2011.

[29] Jacob Perez, Amanda C Maycock, Stephen D Griffiths, Steven C Hardiman, and Christine M McKenna. A new characterisation of the north atlantic eddy-driven jet using two-dimensional moment analysis. *Weather and Climate Dynamics*, 5(3): 1061–1078, 2024.

[30] Sean M Davis and Karen H Rosenlof. A multidiagnostic intercomparison of tropical-width time series using reanalyses and satellite observations. *Journal of Climate*, 25 (4):1061–1078, 2012.

[31] Gareth Berry, Chris Thorncroft, and Tim Hewson. African easterly waves during 2004—analysis using objective techniques. *Monthly Weather Review*, 135(4):1251–1267, 2007.

[32] Clemens Spensberger, Thomas Spengler, and Camille Li. Upper-tropospheric jet axis detection and application to the boreal winter 2013/14. *Monthly Weather Review*, 145(6):2363–2374, 2017.

[33] David Gallego, Pedro Ribera, Ricardo Garcia-Herrera, Emiliano Hernandez, and Luis Gimeno. A new look for the southern hemisphere jet stream. *Climate Dynamics*, 24:607–621, 2005.

[34] Cristina L Archer and Ken Caldeira. Historical trends in the jet streams. *Geophysical Research Letters*, 35(8), 2008.

[35] Francisco J Beron-Vera, María J Olascoaga, Michael G Brown, and Huseyin Koçak. Zonal jets as meridional transport barriers in the subtropical and polar lower stratosphere. *Journal of the atmospheric sciences*, 69(2):753–767, 2012.

[36] Jezabel Curbelo, Carlos R Mechoso, Ana M Mancho, and Stephen Wiggins. Lagrangian study of the final warming in the southern stratosphere during 2002: Part ii. 3d structure. *Climate Dynamics*, 53:1277–1286, 2019.

[37] Gloria L Manney and Zachary D Lawrence. The major stratospheric final warming in 2016: dispersal of vortex air and termination of arctic chemical ozone loss. *Atmospheric Chemistry and Physics*, 16(23):15371–15396, 2016.

[38] George Haller. Lagrangian coherent structures. *Annual review of fluid mechanics*, 47:137–162, 2015.

[39] Clemens Spensberger, Camille Li, and Thomas Spengler. Linking instantaneous and climatological perspectives on eddy-driven and subtropical jets. *Journal of Climate*, 36(24):8525–8537, 2023.

[40] Arnold Gruber. The wavenumber–frequency spectra of the 200 mb wind field in the tropics. *Journal of Atmospheric Sciences*, 32(8):1615–1625, 1975.

[41] BJ Hoskins. Stability of the rossby-haurwitz wave. *Quarterly Journal of the Royal Meteorological Society*, 99(422):723–745, 1973.

[42] Tim Woollings, Camille Li, Marie Drouard, Etienne Dunn-Sigouin, Karim A Elmestekawy, Momme Hell, Brian Hoskins, Cheikh Mbengue, Matthew Patterson, and Thomas Spengler. The role of rossby waves in polar weather and climate. *Weather and Climate Dynamics*, 4(1):61–80, 2023.

[43] Ana M Mancho, Stephen Wiggins, Jezabel Curbelo, and Carolina Mendoza. Lagrangian descriptors: A method for revealing phase space structures of general time dependent dynamical systems. *Communications in Nonlinear Science and Numerical Simulation*, 18(12):3530–3557, 2013.

[44] Brian J Hoskins and Tercio Ambrizzi. Rossby wave propagation on a realistic longitudinally varying flow. *Journal of the Atmospheric Sciences*, 50(12):1661–1671, 1993.

[45] Tim Woollings, Abdel Hannachi, and Brian Hoskins. Variability of the north atlantic eddy-driven jet stream. *Quarterly Journal of the Royal Meteorological Society*, 136 (649):856–868, 2010.

[46] Rachel H White, Casey Hilgenbrink, and Aditi Sheshadri. The importance of greenland in setting the northern preferred position of the north atlantic eddy-driven jet. *Geophysical Research Letters*, 46(23):14126–14134, 2019.

[47] Volkmar Wirth and Christopher Polster. The problem of diagnosing jet waveguidability in the presence of large-amplitude eddies. *Journal of the Atmospheric Sciences*, 78(10):3137–3151, 2021.

[48] Albert Ossó, Ileana Bladé, Alexey Karpechko, Camille Li, Douglas Maraun, Olivia Romppainen-Martius, Len Shaffrey, Aiko Voigt, Tim Woollings, and Giuseppe Zappa. Advancing our understanding of eddy-driven jet stream responses to climate change–a roadmap. *Current Climate Change Reports*, 11(1):2, 2024.

[49] Tiffany A Shaw, Julie M Arblaster, Thomas Birner, Amy H Butler, DIV Domeisen, Chaim I Garfinkel, Hella Garny, Kevin M Grise, and A Yu Karpechko. Emerging climate change signals in atmospheric circulation. *AGU Advances*, 5(6): e2024AV001297, 2024.

[50] Elizabeth A Barnes and Arlene M Fiore. Surface ozone variability and the jet position: Implications for projecting future air quality. *Geophysical Research Letters*, 40(11):2839–2844, 2013.

[51] James A Screen and Ian Simmonds. Exploring links between arctic amplification and mid-latitude weather. *Geophysical Research Letters*, 40(5):959–964, 2013.

[52] Martin S Singh and Paul A O'Gorman. Upward shift of the atmospheric general circulation under global warming: Theory and simulations. *Journal of Climate*, 25 (23):8259–8276, 2012.

[53] JA Madrid and Ana M Mancho. Distinguished trajectories in time dependent vector fields. *Chaos: An Interdisciplinary Journal of Nonlinear Science*, 19(1), 2009.

[54] Carolina Mendoza and Ana M Mancho. Hidden geometry of ocean flows. *Physical review letters*, 105(3):038501, 2010.

[55] Richard T Pierrehumbert and Hong Yang. Global chaotic mixing on isentropic surfaces. *Journal of Atmospheric Sciences*, 50(15):2462–2480, 1993.

[56] Kenneth P Bowman and Gordon D Carrie. The mean-meridional transport circulation of the troposphere in an idealized gcm. *Journal of the atmospheric sciences*, 59 (9):1502–1514, 2002.

[57] Kenneth P Bowman and Tatiana Erukhimova. Comparison of global-scale lagrangian transport properties of the ncep reanalysis and ccm3. *Journal of Climate*, 17(5): 1135–1146, 2004.

[58] Jezabel Curbelo, Víctor José García-Garrido, Carlos Roberto Mechoso, Ana Maria Mancho, Stephen Wiggins, and Coumba Niang. Insights into the three-dimensional lagrangian geometry of the antarctic polar vortex. *Nonlinear Processes in Geophysics*, 24(3):379–392, 2017.

Acknowledgments

Thanks to Penelope Maher and Talia Tamarin-Brodsky for enlightening discussions during the preparation of the manuscript, and to Anika Hatzius for assistance during an internship. Computations were run on the Cannon cluster at Harvard and the Svante HPC at MIT.

Funding:
International Program for Research Groups (IP4RG), Centre de Recerca Matemàtica at Universitat Autònoma de Barcelona (LR, JC)
Agencia Estatal de Investigación RYC2018-025169, PID2020-114043GB-I00, PID2021-122954NB-I00, CEX2020-001084-M, CNS2023-144360 (JC)
Fundación Ramón Areces (JC)
Fundación BBVA (JC)
William F. Milton Fund (LR, ML)
Harvard Solar Geoengineering Research Program (ML)

Competing interests:
Authors declare that they have no competing interests.

Data and materials availability:
The JetLag dataset is available at DOI tbd on Zenodo.

Author contributions

Conceptualization: LR, JC, ML
Methodology: LR, JC
Investigation: LR, JC
Visualization: LR
Writing—original draft: LR, JC
Writing—review & editing: LR, JC, ML